

# Characterizing wind turbine drivetrain nonlinearities for hybrid nacelle tests

**Siddiqui, Muhammad Omer; Guo, Yi; Nejad, Amir R.; Wenske, Jan**

*Published in:*
Forschung im Ingenieurwesen

*Link to article, DOI:*
10.1007/s10010-025-00817-y

*Publication date:*
2025

*Document Version*
Publisher's PDF, also known as Version of record

Forschung im Ingenieurwesen (2025)89:39
https://doi.org/10.1007/s10010-025-00817-y

ORIGINALARBEITEN/ORIGINALS

# Characterizing wind turbine drivetrain nonlinearities for hybrid nacelle tests

**Muhammad Omer Siddiqui[1,2] · Yi Guo[3] · Amir R. Nejad[2] · Jan Wenske[1]**

Received: 24 September 2024 / Accepted: 14 February 2025


**Abstract**
The increasing size of modern wind turbines presents significant challenges to existing nacelle testing infrastructures that are unable to reproduce the required extreme loads, achieve the necessary dynamic load bandwidth and provide increased power capacity while maintaining escalating costs of testing. The novel hybrid nacelle testing approach developed at Fraunhofer IWES aims to resolve some of these challenges. It combines high-fidelity virtual models with partial load physical testing to predict full load responses on a nacelle test bench. One of the primary challenges related to this new testing approach is ensuring that the underlying models accurately capture the complex nonlinear interactions and behaviors that can occur under full load conditions. This paper investigates the sources of nonlinearities in the response of the drivetrain during steady-state parasitic load tests on a nacelle test bench. Multiple system responses are investigated, and the corresponding type of nonlinearity is classified. A full understanding of these critical nonlinearities in the system will enable the development of a suitable modeling approach and partial test criteria required to perform hybrid nacelle testing.

## 1 Introduction

The wind energy sector has witnessed substantial advances towards finding alternatives to field testing in recent years, leading to the development of several ground-based nacelle testing facilities around the world [1]. These facilities offer system-level testing capabilities for the entire nacelle in a controlled and repeatable environment, and can reproduce various field-like drivetrain responses [2–4]. Advanced nacelle test benches, equipped with technologies like artificial grid simulators and hardware-in-the-loop setups, can even facilitate electrical certification testing [5]. These facilities have become an attractive method for testing, as they enable manufacturers to address potential design flaws early on, reducing the risk of costly delays and setbacks during field testing and certification. Some of the individual tests that can be conducted during a nacelle test campaign are listed in Table 1.

Despite their advancements, nacelle test benches are facing several challenges to keep up with the growing testing demands of modern wind turbines, which are continuously increasing in size and power capacity. The existing nacelle testing infrastructures are unable to reproduce the demanded extreme loads, achieve the necessary dynamic load bandwidth, and provide increased power capacity while maintaining escalating costs of testing [1]. The rapid evolution of wind turbine technology necessitates corresponding advancements in nacelle testing methodologies. While there is a growing trend towards larger nacelle test benches to accommodate the increasing size of wind turbines [1], this approach may not be the most sustainable or cost-effective long-term solution. Additionally, constructing even larger test benches with possibly higher test costs associated with them can create significant barriers to entry for smaller wind turbine manufacturers, limiting their ability to utilize these facilities and hindering their development process [6]. Consequently, innovations are required to enhance the utilization of existing nacelle test benches.

The novel hybrid nacelle testing approach developed at Fraunhofer IWES aims at resolving some of the aforementioned challenges [7]. The proposed hybrid testing for wind turbine nacelles, as elaborated in Fig. 1, is a systematic

✉ Muhammad Omer Siddiqui
muhammad.omer.siddiqui@iwes.fraunhofer.de

1 Fraunhofer Institute for Wind Energy Systems IWES, Am Luneort 100, 27572 Bremerhaven, Germany

2 Department of Marine Technology, Norwegian University of Science and Technology, NO-7491, Trondheim, Norway

3 DTU Wind Energy, Frederiksborgvej 399, 4000 Roskilde, Denmark

Published online: 26 February 2025

**Table 1** Typical mechanical and electrical tests conducted on a nacelle testing bench [1]

| Mechanical tests | Electrical tests |
|---|---|
| Modal analysis | Fault ride through tests |
| Acoustic noise and vibration | Control performance |
| Speed and torque ramp-up | Frequency variations |
| Heat run | Flicker tests |
| Lubrication tests | Grid impedance |
| Parasitic loads | Harmonic injection |
| Shock tests | Power quality |

procedure for testing larger wind turbine nacelles on a test bench with a smaller testing capacity. It utilizes a high-fidelity virtual model of the device under test (DUT) and the test bench for the prediction of responses of the DUT beyond the load application capacity of the test bench. First, full-scale physical tests are conducted on a nacelle test bench at partial loads that are achievable within the load application capability of the test bench. Alongside these tests, virtual testing is performed for the same load regime. The measured response of the DUT at partial loads, obtained from physical tests, is compared against the simulation results from virtual tests, and the virtual model is adapted as necessary to achieve the desired accuracy. The virtual model of the nacelle is validated using only the partial load response obtained during the physical testing. Afterward, the validated virtual model is used to simulate the response of the DUT under full loads beyond the testing limits of the test bench. Unlike scaled testing, this approach removes the uncertainties that are inherent to a physical scaling of the test specimen. This novel approach has demonstrated promising results for some of the responses of the DUT in the case of non-torque load tests [8].

Since partial load data is used to validate the simulation models, the expected shape of the nonlinear response trend at full load needs to be correctly predicted by the virtual model itself. This is particularly challenging for hybrid nacelle testing, as nonlinearities, if not correctly modeled, can introduce uncertainty in the predicted full load system response [9]. The intensity of nonlinear effects can also differ between partial and full load conditions, which further com-

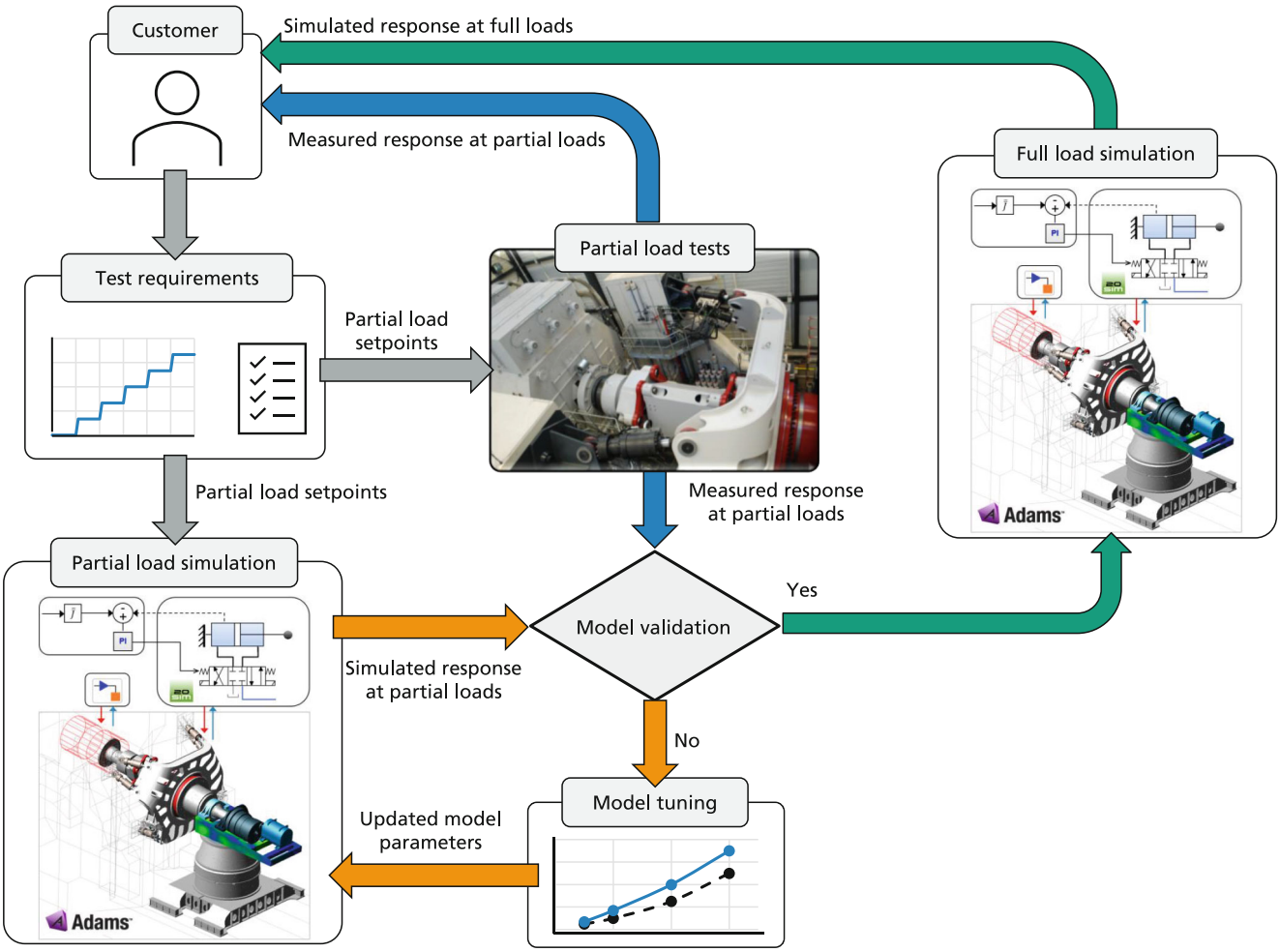


**Fig. 1** Schematic representation of the hybrid nacelle testing methodology [8]

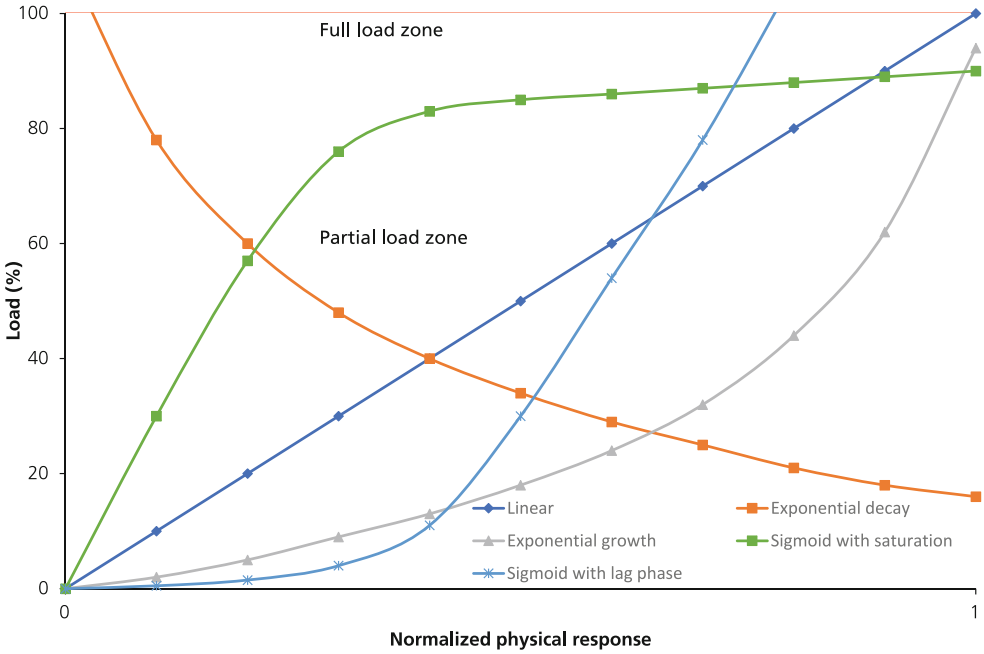


**Fig. 2** Possible shapes of system response across different load regions

plicates the model tuning process. Figure 2 illustrates some of the possible nonlinear response patterns that can appear across different load regions. Nonlinear system behaviors, like sharp sigmoidal transitions and exponential increases and decreases, pose significant challenges for hybrid nacelle testing. This is because the successful implementation of hybrid testing is highly dependent on accurate representation of such nonlinear behaviors in the virtual models [9].

Comprehensive understanding of the system's nonlinear behavior across various load conditions is therefore crucial for developing effective modeling techniques that support the successful implementation of hybrid nacelle testing. This paper investigates the characteristics of nonlinear behavior in drivetrains during nacelle testing. Case studies are conducted using unidirectional load tests on a multi-megawatt drivetrain to various responses such as vibrations, deflections, deformations, and loads. The resulting load-response data is analyzed to identify and characterize different types of nonlinear behavior. A comprehensive understanding of these critical nonlinearities will pave the way for the development of appropriate modeling approaches essential for the successful implementation of hybrid nacelle testing.

The paper is organized as follows: Section 2 outlines the research methodology, including the test setup and measurement techniques utilized in the case studies presented in this paper. Section 3 showcases the results obtained from these case studies. Section 4 discusses key observations and insights derived from the presented results. The paper ends with the conclusion in Sect. 5.

## 2 Methodology

### 2.1 Experimental testing of a 5 MW nacelle

Figure 3 illustrates the key components of the DyNaLab (Dynamic Nacelle Testing Laboratory) and the DUT during nacelle testing at Fraunhofer IWES. The DyNaLab is capable of electrical and mechanical tests for wind turbine nacelles. It features a hexapod load application system (LAS) driven by six servo-hydraulic actuators, capable of applying bending moments up to 20 MNm and thrust and shear forces up to 2 MN. The test bench drive system consists of two motors coupled in tandem to transmit rotational motion and torque to the DUT, with a nominal power of 10 MW at 11 rpm. A flexible coupling ensures that only torque loads are transmitted from the motors to the DUT, while a torque limiter safeguards the drive system by disconnecting the motor shaft and coupling in case of excessive torque levels. The test bench drive system is inclined at a 5° angle from the horizontal axis to replicate the typical inclination of a wind turbine nacelle.

In the presented work, Nacelle tests are used on a GE Vernova 5 MW platform conducted at the DyNaLab. The nacelle DUT incorporates a multi-stage geared high-speed drivetrain with a three-point suspension topology. A double-row spherical roller bearing (SRB) serves as the main bearing, connecting the main shaft to the gearbox's first planet carrier via a shrink disc. The gearbox is mounted on a support structure through an array of bolts with special elastomers to accommodate deflections under various loads. A flexible coupling connects the gearbox to the generator, accommodating any misalignments. The entire nacelle sys-

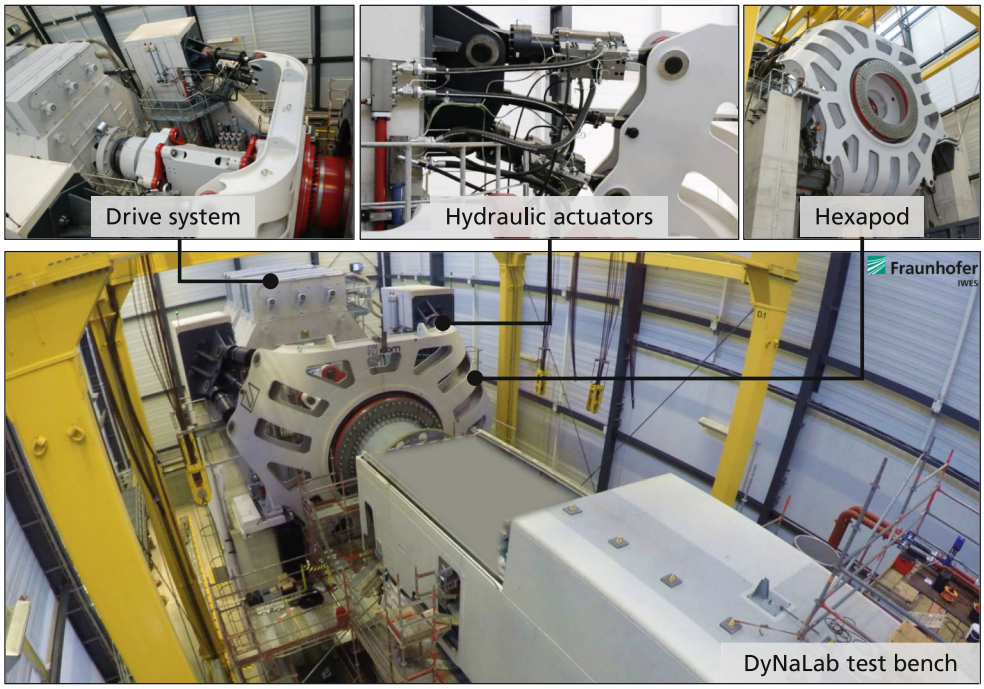


**Fig. 3** Main features of the DyNaLab during testing of the 5 MW nacelle system

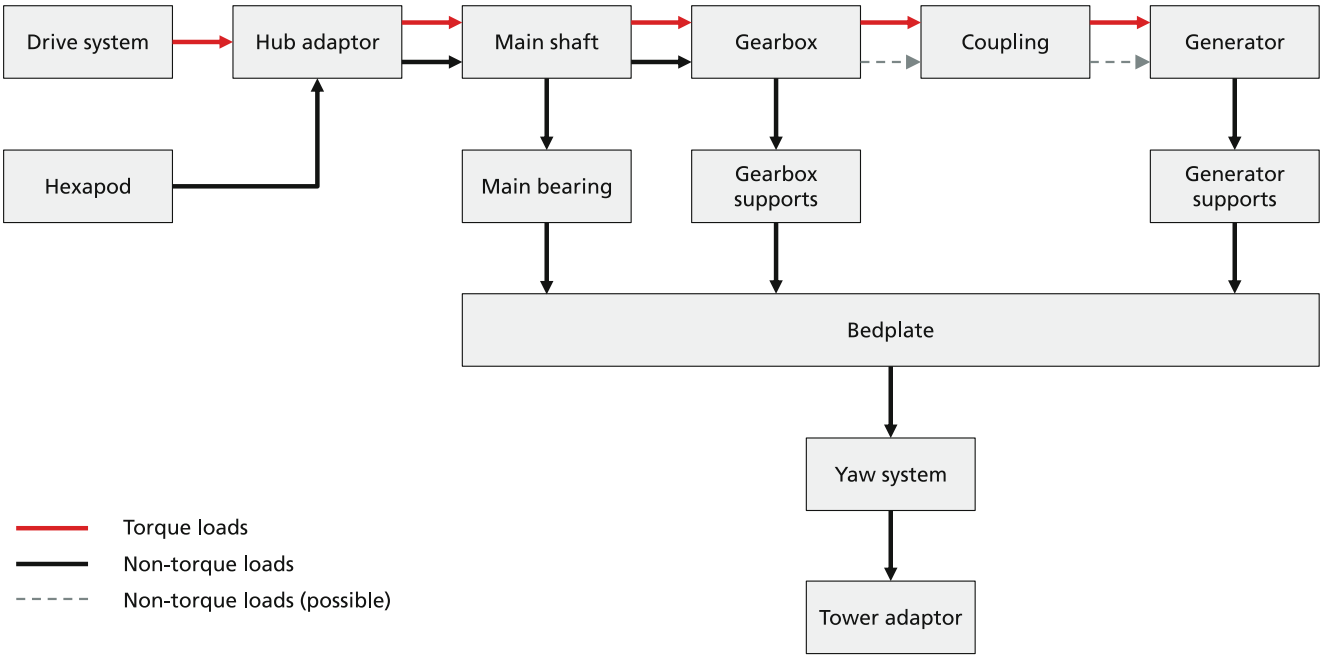


**Fig. 4** Theoretical load transfer path during nacelle testing

tem rests on the tower adapter at the yaw bearing interface, with the yaw system locked to prevent nacelle motion in the yaw direction.

Figure 4 shows the load transfer path from the LAS of the test bench to the DUT during nacelle testing. The rotor loads can take different paths through various mechanical components that have nonlinear properties because of their internal structure, which can divide the loads on subsequent paths or influence neighboring components by their nonlinear relationship between load and deformation [10]. In this type of drivetrain topology, the non-torque rotor loads are supported by the main bearing and the gearbox support structure [11]. The majority of the non-torque loads are transmitted to the bedplate via the main bearing. The non-torque loads entering the gearbox act on the planet carrier of the first gear stage and are transmitted via the planet carrier

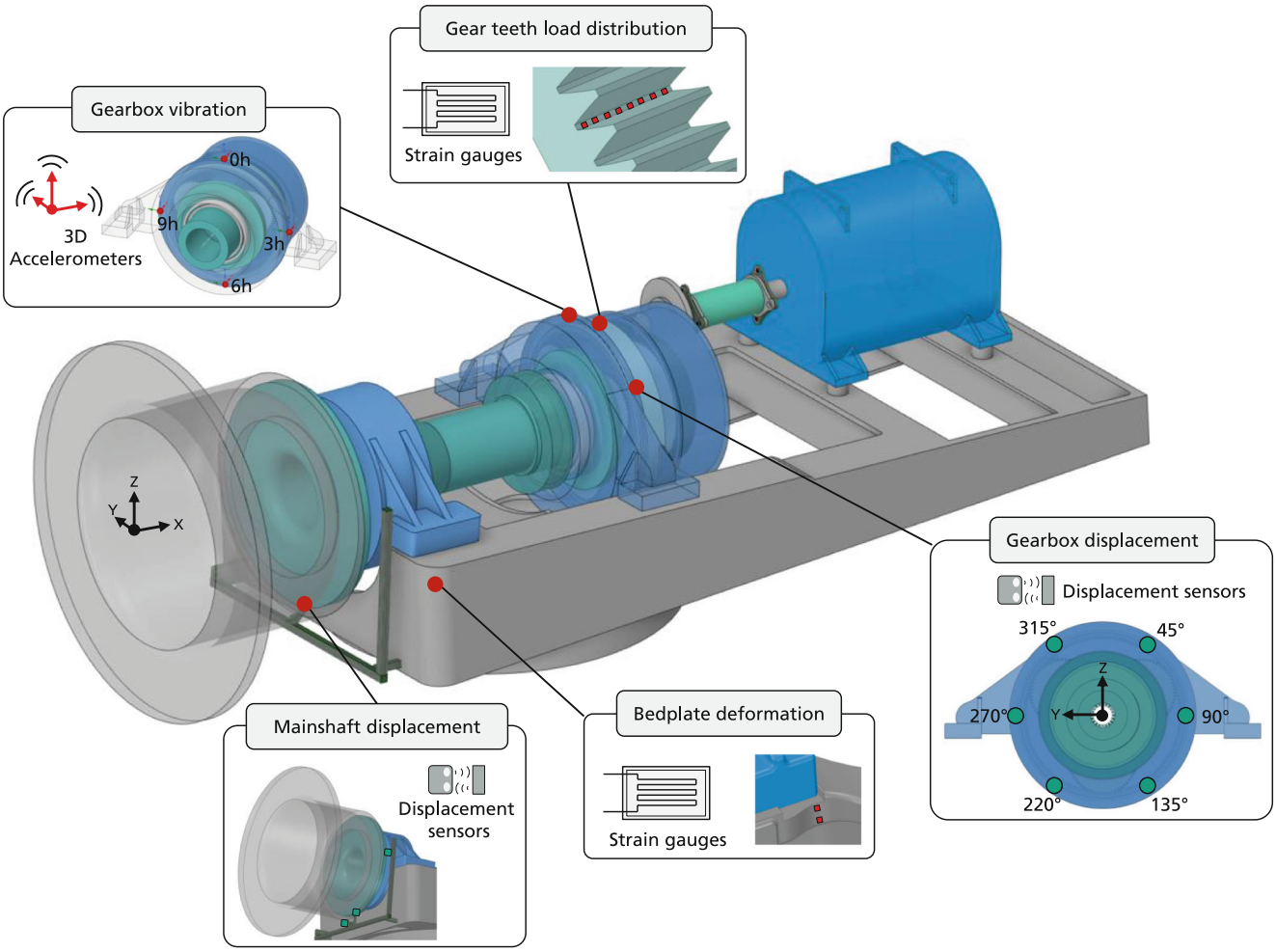


**Fig. 5** Sensor types and locations on the DUT for measuring the responses of interest. (The design of the actual drivetrain may differ from the depicted illustration)

bearings into the gearbox housing. Due to relative clearance and stiffness characteristics in relation to planet bearings, the planet bearings (and hence the planets) may also react an appreciable amount of non-torque loads [12, 13]. The non-torque loads entering the gearbox consequently travel through the gearbox support structure into the bedplate.

## 2.2 Measurement systems

In the scope of the present work, the following system responses are in focus;

- Mainshaft deflections
- Gearbox deflections
- Gear flank load distribution
- Gearbox vibrations
- Bedplate deformation

This requires installation of sensors of various types on multiple locations of the drivetrain, as depicted in Fig. 5. Laser sensors are installed in close proximity to the main bearing to measure the relative displacement between the main shaft and the bedplate in axial, lateral, and vertical directions. Multiple laser sensors are installed between the gearbox housing and its support structure to measure the gearbox housing deflections relative to the support structure in axial, lateral, and vertical directions.

To measure the bedplate deformation due to applied loads, strain gauges are installed at multiple locations, typically where higher stress concentrations and hot-spots are expected to occur.

The gearbox is also instrumented with high-precision, three-axis accelerometers at multiple locations to fully capture its vibration response. The vibrations recorded by the accelerometers are used to calculate the root mean square (RMS) values corresponding to each load level.

Strain gauges are installed on the ring gear to measure gear flank strain distribution across the gear-face width. For a given pair, gear stress (and hence gear life) critically depends on load distribution across the face. The gear face load distribution factor ($K_{H\beta}$) is one of the most important

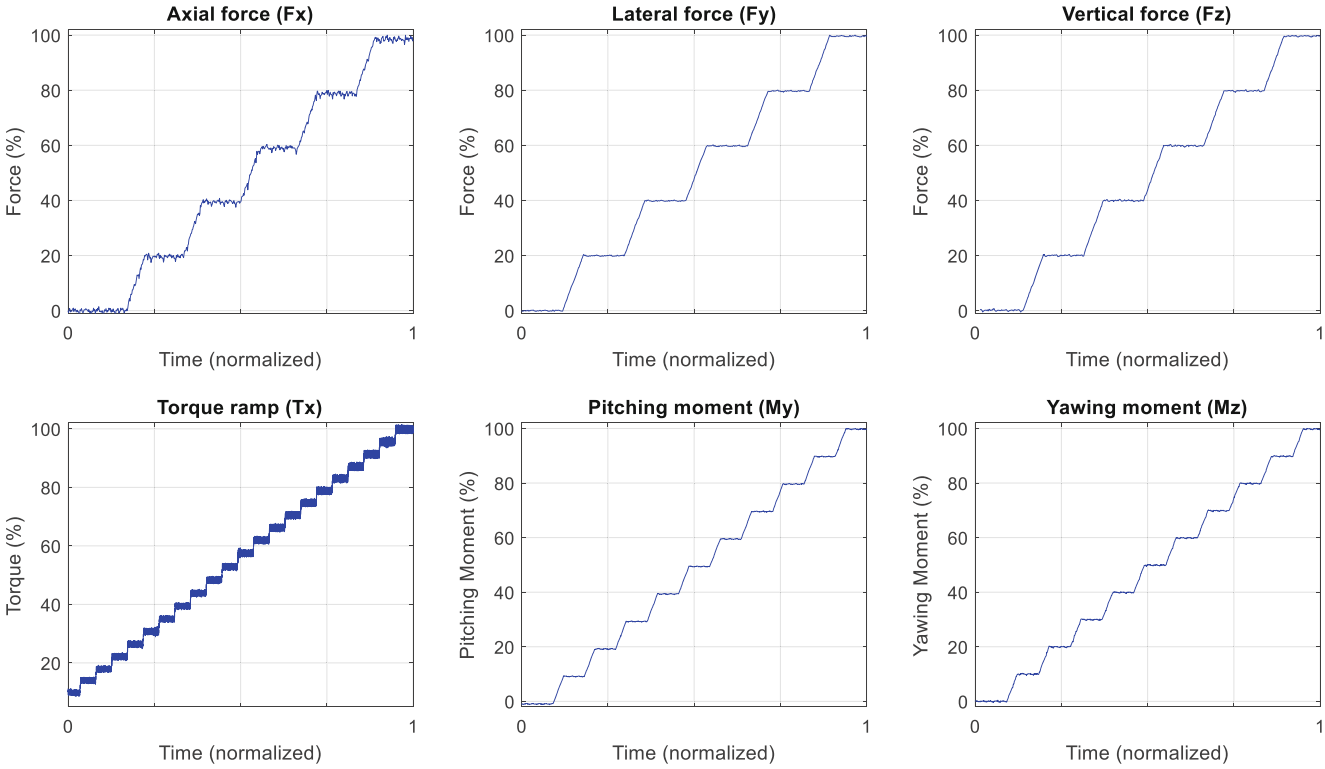


**Fig. 6** Stepped forces, moments and torque applied on the DUT during nacelle testing

items for a gear strength calculation as it quantifies the non-uniformity of the load distribution on the gear flank. It is defined by the ISO 6336-1 [14] as:

$$K_{H\beta} = \frac{\text{Maximum load per unit face width}}{\text{Average load per unit face width}} = \frac{\left(\frac{F}{b}\right)_{\max}}{\frac{F_m}{b}} \quad (1)$$

In an idealized gear pair, the load is evenly distributed across the contact face. High values of ($K_{H\beta}$) are normally associated with eccentric loading of gears. For measuring the gear face load distribution, the gear root strain distribution ($K_{\varepsilon\beta}$) can be calculated which can later be converted into the flank load distribution ($K_{H\beta}$) [15];

$$K_{\varepsilon\beta} = \frac{\text{Maximum strain per unit face width}}{\text{Average strain per unit face width}} = \frac{\left(\frac{\varepsilon}{b}\right)_{\max}}{\frac{\varepsilon_m}{b}} \quad (2)$$

In the present study, all the calculations for $K_{\varepsilon\beta}$ are based on a first planetary stage of the DUT. The strain gauges are installed at the bottom of the tooth where the deformations are not maximum, but are large enough to take readings and do not present as much variability due to positioning errors. It is important to mention that since the ring gear is a static component, the strain distribution captured by an instrumented gear tooth in the ring gear is position dependent. With eight strain gauges on the ring gear tooth, the peak-to-peak values for individual mesh events were used to generate load distribution patterns. Afterwards, the mesh distribution of the averaged peak-to-peak values of each individual strain gauge was used to calculate the gear root strain distribution ($K_{\varepsilon\beta}$) at each load level.

## 2.3 Test cases

The considered test cases involve the test bench applying the following stepped loads in steady-state to the drivetrain:

- Axial forces ($F_x$)
- Lateral forces ($F_y$)
- Vertical forces ($F_z$)
- Torque ($T_x$)
- Pitching moment ($M_y$)
- Yawing moment ($M_z$)

Stepped loads are applied at the hub interface with increasing amplitude for each of the aforementioned load directions (as shown in Fig. 6). The load amplitudes have been normalized with 100% depicting the maximum load that was applied during tests. In each test, the stepped loads are applied in one direction at a time. This type of test helps identify the structural stiffness of the DUT components in the corresponding load directions. During these tests, the DUT was operating at nominal speed.

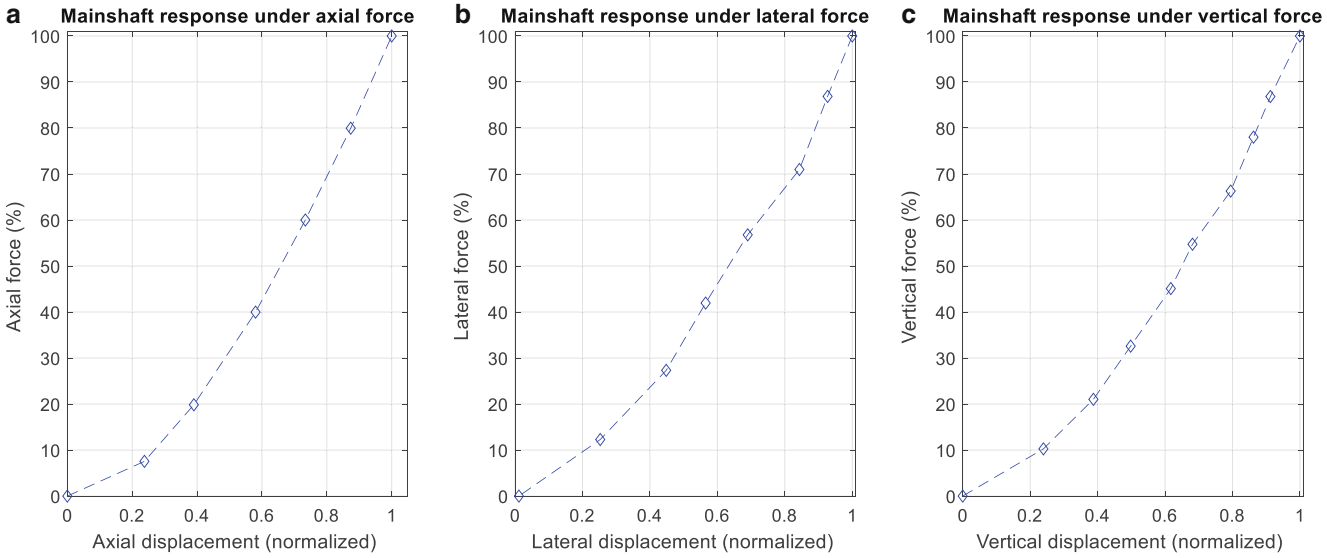


**Fig. 7** Mainshaft deflection under axial (**a**), lateral (**b**), and vertical force (**c**)

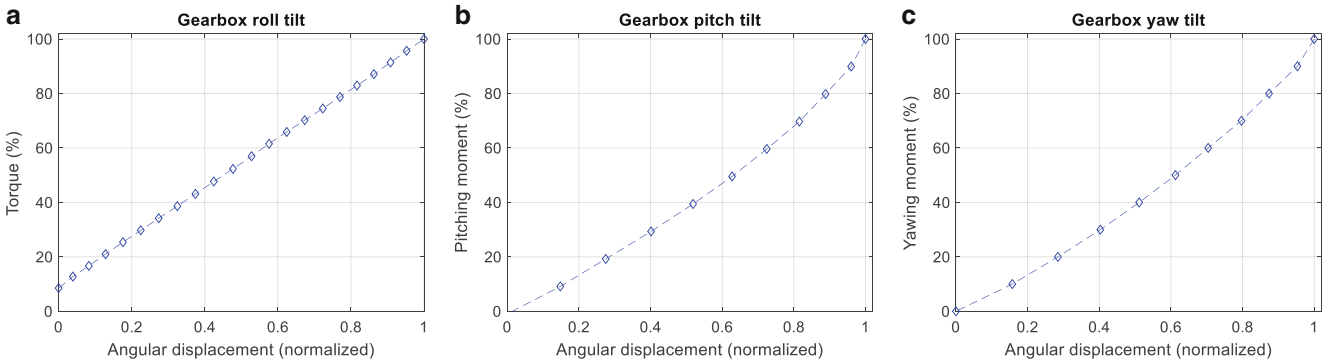


**Fig. 8** Gearbox roll tilt with increasing torque (**a**), pitch tilt with increasing pitching moment (**b**), and yaw tilt with increasing yawing moment (**c**)

## 3 Results

### 3.1 Mainshaft deflection

The SRB type main bearing is capable of withstanding high radial and axial loads, and its self-aligning capability prevents the build-up of reaction moments. However, these types of bearings have operational clearance, which depends on the manufacturing tolerances, mounting conditions, temperature distribution of the bearing, and hub loads that can introduce nonlinearities. The displacements of the main shaft under applied forces in different directions are plotted in Fig. 7. The experimentally measured response has higher nonlinearity in the lower load regions compared to the full load region. The main shaft shows a higher rate of displacement at lower loads in relation to the higher load region. This can be attributed to the main bearing, which initially makes a rigid body motion inside the clearance region until the rollers come into contact. Bearings with a significant amount of clearance might exhibit an exponential growth curve with a more pronounced initial curved portion due to the gradual contact between the rolling elements and the raceways. At higher loads, the gradient increases, which signifies the stiffening effect of the rollers.

### 3.2 Gearbox deflections

The gearbox is bolt-connected to the support structure, with special elastomers forming a crucial part of each bolted connection. This bolted interface with elastomers primarily supports the torque loads, accommodates misalignment, provides noise and vibration isolation, and protects from shock loads. The stiffness of the gearbox elastomer has a stronger influence on the deflection of the gearbox housing. Severe gearbox deflections can significantly affect the alignment of the gearbox and generator. The deflections of the complete gearbox with respect to the support structure under different load directions are plotted in Fig. 8. It can be observed that the gearbox roll tilt increases with applied torque in a linear fashion. However, the angular deflections

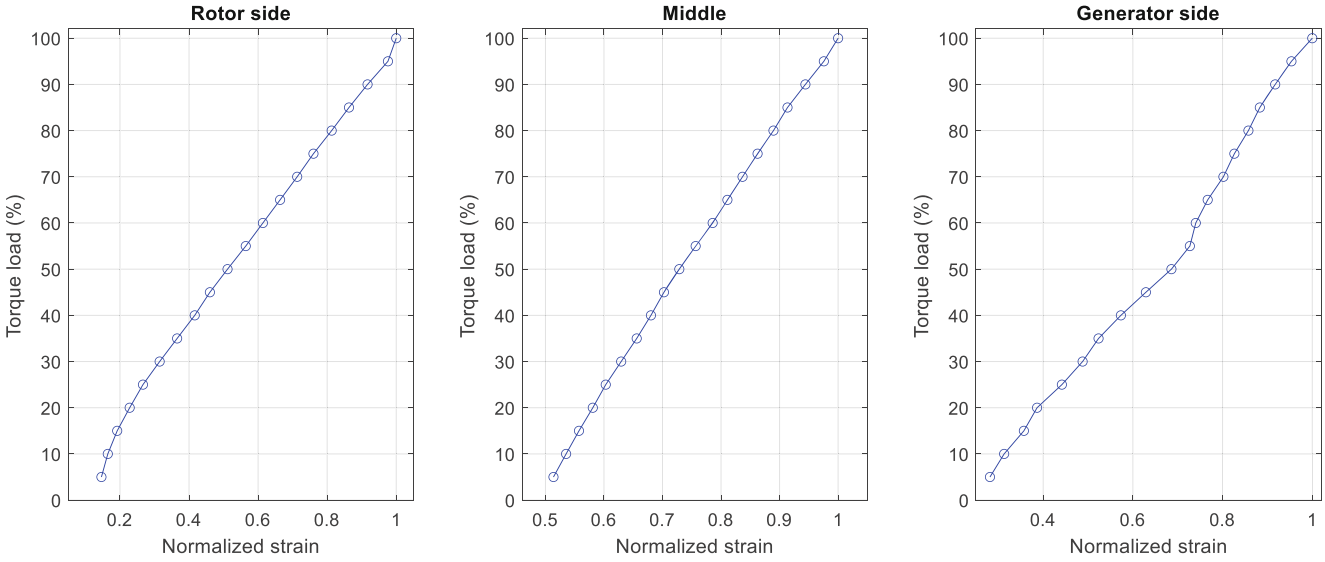


**Fig. 9** Gear flank strain with increasing torque

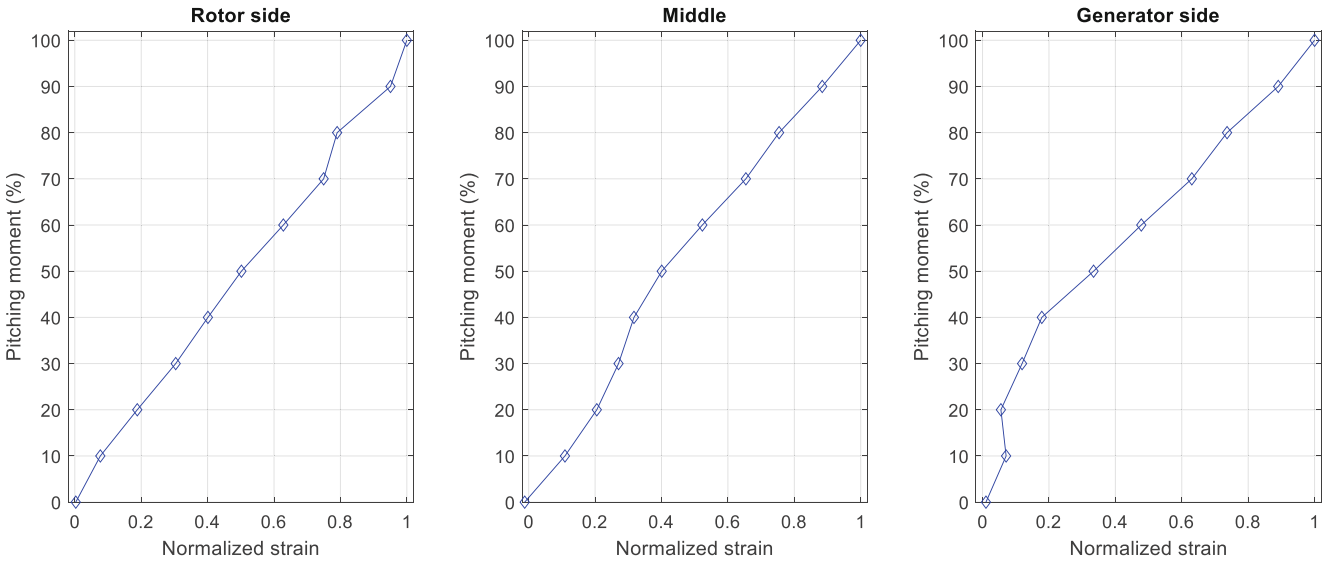


**Fig. 10** Gear flank strain with increasing pitching moment

of the gearbox under pitching moments and yawing moments are observed to be nonlinear. In both of these cases, the gearbox initially tilts at a higher rate below the 40% load zone. After 50% load zone, the gearbox tilting rate becomes slower. This could be linked to the stiffening effect of the elastomers in the bolted connection.

## 3.3 Gear loads

The relative strain values, plotted against the increasing torque loads and pitching moments, are shown in Fig. 9 and Fig. 10 respectively. The rotor side corresponds to the strain gauge installed at the extreme left part of the gear teeth flank, and the generator side corresponds to the extreme right. In the case of stepped torque loads, the middle part of the gear flank shows a linear relationship between strain and applied torque, whereas the edges show a nonlinear trend. In the case of pitching moments, the nonlinearity becomes more prominent in the strain measurements at the generator side.

Figure 11 shows the calculated gear root strain distribution for the case of torque ramp test and pitching moments. Reduction in $K_{\varepsilon\beta}$ is observed as the torque increases, which suggests improvement in load sharing across the tooth contact area. The relationship of $K_{\varepsilon\beta}$ versus applied torque resembles an exponential decay. At higher torque, $K_{\varepsilon\beta}$ decreases at a slower rate, whereas at lower torque, $K_{\varepsilon\beta}$ decreases at a higher rate.

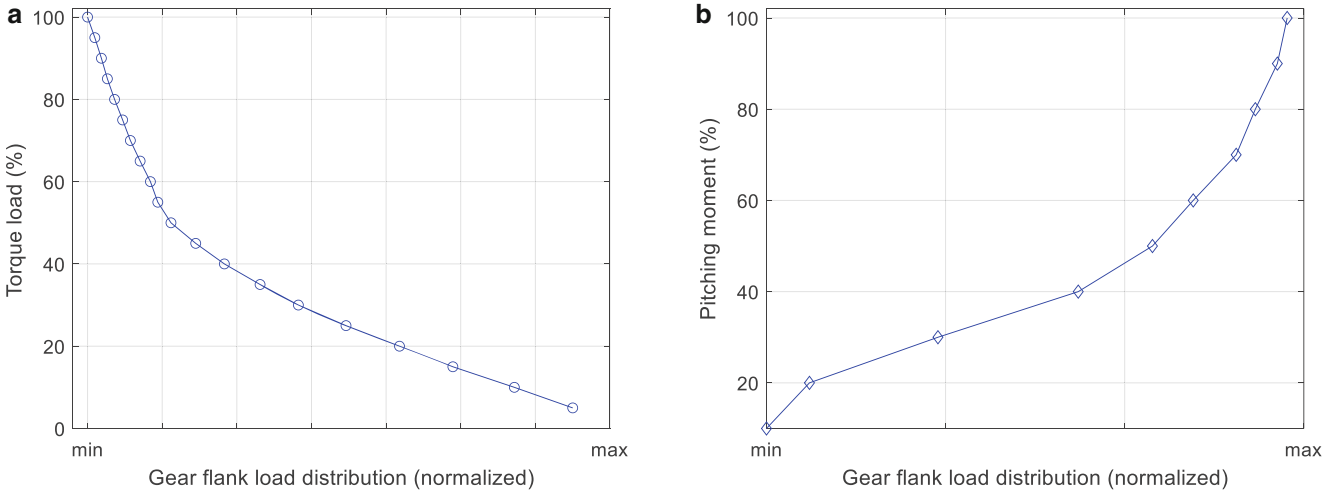


**Fig. 11** Ring gear flank load distribution as a function of applied torque (**a**) and as a function of increasing pitching moment (**b**)

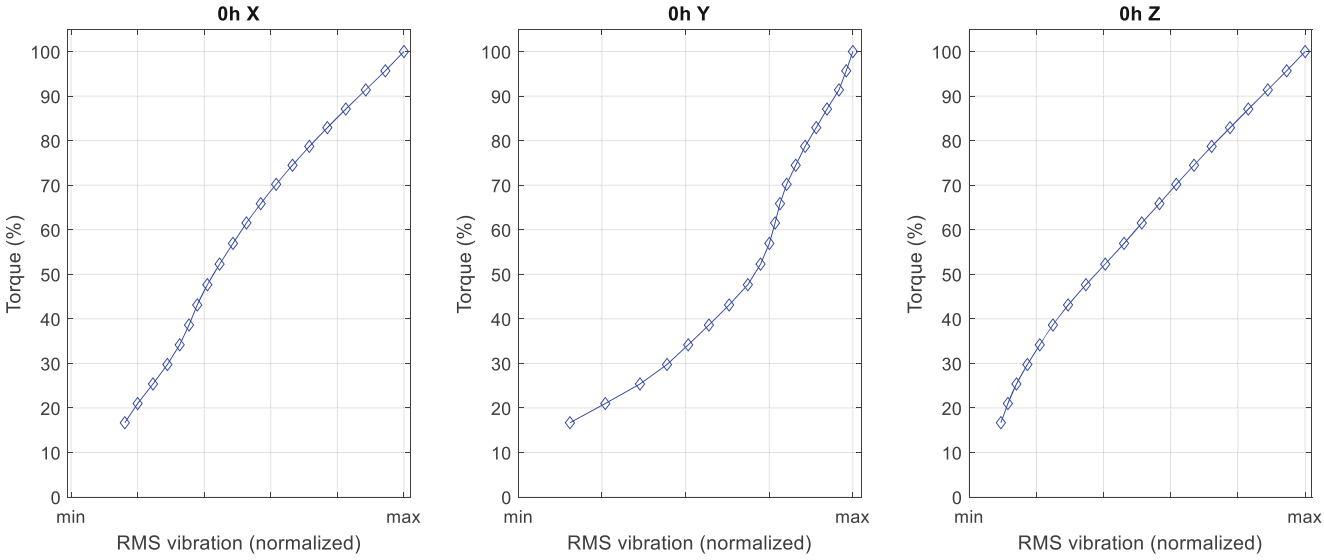


**Fig. 12** Gearbox vibrations versus increasing applied torque in multiple directions

For the case of pitching moments, the curve takes the exact opposite shape where $K_{\varepsilon\beta}$ increases as the applied pitching moments increase. Furthermore, $K_{\varepsilon\beta}$ increases at a rapid rate below 40% load zone. After 50% load zone, $K_{\varepsilon\beta}$ increases at a slower rate. This trend in $K_{\varepsilon\beta}$ has a direct correlation with the observed deflection of the gearbox under applied pitching moments (shown in Fig. 8). Higher pitch and yaw tilting of the gearbox leads to more non-torque entering the gears, which eventually disrupts the gear load distribution.

### 3.4 Gearbox vibrations

The vibrations measured on the gearbox housing are highly nonlinear. Overall, gearbox vibration amplitudes increase with applied torque at each sensor location and in all measured directions. Figure 12 shows the gearbox vibrations for the sensor located at the top of the first gear stage under the torque ramp. The vibration response shows nonlinear behavior that is different in the axial, vertical, and lateral directions. In the axial direction, the vibrations in partial load zones increase at a slower rate and more rapidly in the full load range (resembling a sigmoid curve with saturation). However, the gearbox vibration response trend for the lateral direction resembles an exponential growth curve. For the vertical direction, the vibrations increase in an almost linear fashion. When compared with $K_{\varepsilon\beta}$ versus applied torque (shown in Fig. 11), it can be observed that after the 50% applied torque region, the rate of change of $K_{\varepsilon\beta}$ as well as the vibration amplitude changes. This highlights a strong correlation between the gear load distribution and the resulting gear vibrations.

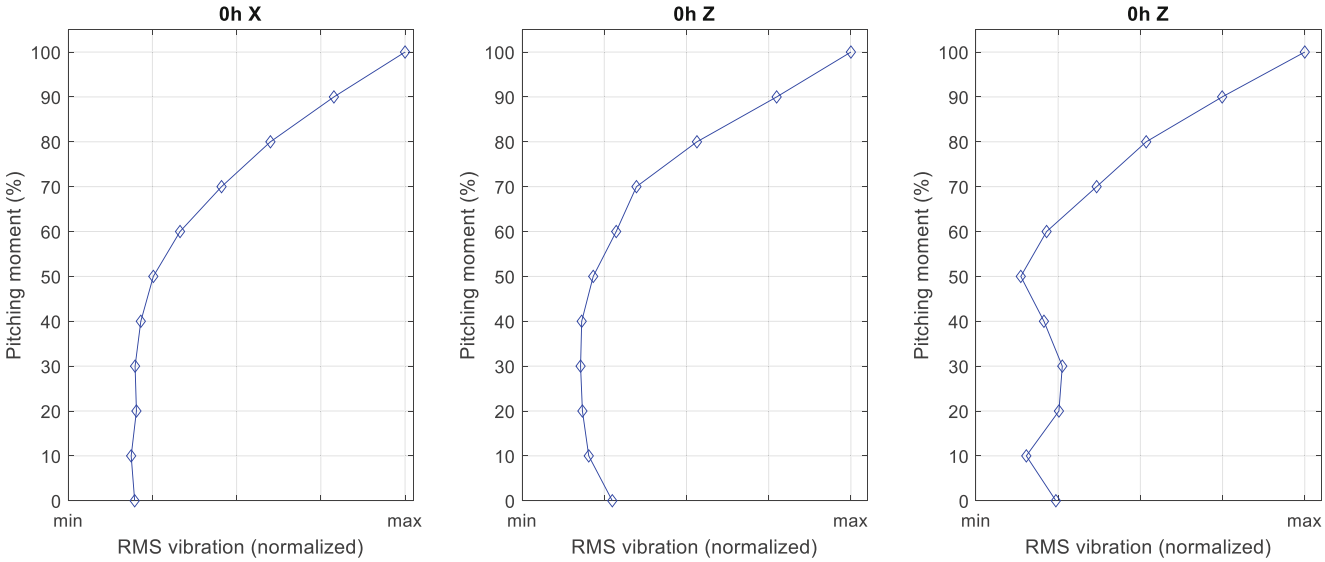


**Fig. 13** Gearbox vibrations versus increasing pitching moment at multiple directions

Figure 13 shows the gearbox vibrations for the sensor located at the top of the first gear stage under the pitching moments. When applying pitching moments, for most of the measurement points, very small changes are observed in the vibrations in the partial load zones. In full load zones, the vibrations increase rapidly with increasing pitching moments. This could be due to higher non-torque loads entering the gearbox due to increasing gearbox tilting. The trends are similar in all three measured directions, resembling the shape of a sigmoid curve with saturation.

### 3.5 Bedplate deformation

The analysis of bedplate deformation under various parasitic loads is also a response of interest during nacelle testing, as it allows investigation of possible stress concentration zones (also known as hot-spots) for design evaluation. The strain measured at hot-spot regions on the bedplate shows a linear relationship with the applied loads in all loading directions (see Fig. 14). There are multiple locations on the bedplate for analyzing the hot-spots, and they all show similar strain response. Such linearity in the actual system response is relatively easier for the model to predict the full load response with less uncertainty. In a previously conducted sensitivity study, it was observed that the stiffness of the main bearing (which is nonlinear) has a noticeable effect on the strain readings at the strain gauge location on the bedplate for the pitch loads [8]. Still, the bedplate strain response shows a linear relationship with the applied loads.

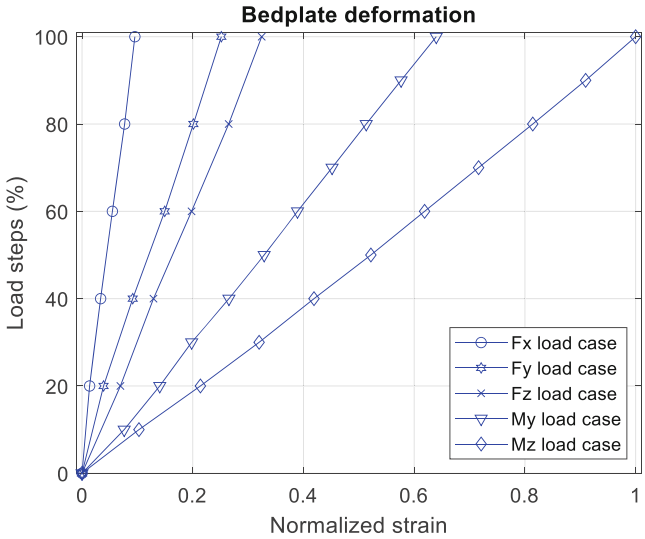


**Fig. 14** Strain response close to a hot-spot corner of the bedplate under various load directions

## 4 Discussion

Several drivetrain responses exhibit nonlinear behavior, as exemplified in the presented case studies. It is favorable for the hybrid testing method when the physical responses of interest exhibit higher nonlinearities in partial load regions and lower nonlinearities in full load regions. This has the advantage that the highly nonlinear response regions are covered by the partial load tests, and the virtual model only has to predict the full load response where fewer nonlinearities are expected. For cases where higher nonlinearities are anticipated in full load regions, the model must be developed to accurately simulate this behavior. Having the

**Table 2** Characterization of the observed drivetrain responses during testing of the 5 MW drivetrain

| Response | Load case | Response curve type | Response characteristic | |
|---|---|---|---|---|
| | | | Partial load zone | Full load zone |
| Mainshaft displacement | Axial load | Exponential growth | Rapid increase | Slower increase |
| | Lateral load | Exponential growth | Rapid increase | Slower increase |
| | Vertical load | Exponential growth | Rapid increase | Slower increase |
| Gearbox roll tilt | Torque | Linear | Constant increase | Constant increase |
| Gearbox pitching tilt | Pitching moment | Exponential growth | Rapid increase | Slower increase |
| Gearbox yawing tilt | Yawing moment | Exponential growth | Rapid increase | Slower increase |
| Gear flank load distribution | Torque | Exponential decay | Rapid increase | Slower increase |
| | Pitching moment | Exponential growth | Rapid increase | Slower increase |
| Gearbox vibration X | Torque | Sigmoid with saturation | Slower increase | Rapid increase |
| Gearbox vibration Y | Torque | Exponential growth | Rapid increase | Slower increase |
| Gearbox vibration Z | Torque | Linear | Constant increase | Constant increase |
| Gearbox vibration X | Pitching moment | Sigmoid with saturation | Constant | Rapid increase |
| Gearbox vibration Y | Pitching moment | Sigmoid with saturation | Constant | Rapid increase |
| Gearbox vibration Z | Pitching moment | Sigmoid with saturation | Constant | Rapid increase |
| Bedplate deformation | Forces | Linear | Constant increase | Constant increase |
| | Moments | Linear | Constant increase | Constant increase |

knowledge of expected trends of the nonlinear responses of the drivetrain system can help in developing appropriate nonlinear virtual models. This study is an attempt to build this knowledge of nonlinear system response for a specific type of drivetrain. Table 2 summarizes the key findings regarding the nonlinear responses analyzed in this work.

The mainshaft displacements showed higher nonlinearity in the partial loads as compared to the full load region. This also agrees with findings of other cases studies conducted on SRB type main bearings [16, 17]. The gradual increase of loads progressively increases the rolling element force as more rolling elements are in contact under higher loads, leading to a progressive increase in stiffness [16]. This is because the main bearing stiffness is a function of the contact state of the rollers under the applied radial and axial loads [17]. This type of nonlinear behavior can be effectively modeled in simulation by incorporating nonlinear bearing stiffness [8].

The gearbox roll tilt under the application of stepped torque loads exhibited a linear relationship. The linear behavior of the elastomers can be modeled with bushing elements [8]. In contrast, the gearbox pitching and yawing tilts showed exponential curves with higher nonlinearity at full loads. This will be more challenging and will require nonlinear force elements to capture these effects.

Gear flank load distribution demonstrated an exponential decaying trend with increasing torque loads and an exponential growth trend with increasing pitching moments. Such gear teeth strain response requires more advance modeling approach with high-fidelity gear teeth contact models [18].

Gearbox vibrations, in most locations and directions, displayed sigmoid-shaped or exponential growth responses. This nonlinear behavior necessitates a comprehensive understanding and accurate modeling of the entire load transfer path. Furthermore, responses such as gear flank load distribution and gear vibrations are influenced not only by detailed gear and gear contact models but also by the global displacements of the planet carrier and shafts [18–20]. Such responses, which exhibit significant changes in trend within the full load region compared to the partial load region, can complicate model validation solely based on partial load measurements.

The bedplate deformation identified by measuring the strains in the critical hot-spot regions showed a linear behavior for all load cases. The bedplate deformation can be captured well with conventional finite-element based flexible body with appropriate mesh density [8].

Beyond identifying a suitable modeling approach, understanding the nonlinear drivetrain responses is also essential for defining the optimal partial load tests for hybrid testing. Accurate determination of the partial load range is critical for correctly tuning and validating the virtual model, ensuring its effectiveness in predicting the full-load behavior. Future work will focus on establishing criteria for defining appropriate partial load limits based on the specific characteristics of the observed nonlinearities.

## 5 Conclusion

The successful implementation of hybrid nacelle testing depends on accurately modeling the nonlinear behavior of the

drivetrain. This study aimed to characterize the nonlinear response in the drivetrain to gain a comprehensive understanding of the critical nonlinearities. This is essential for developing appropriate modeling approaches to support the successful implementation of hybrid nacelle testing. The paper analyzed the mechanical responses of a 5 MW wind turbine drivetrain under steady-state stepped loads applied in multiple directions. Using the measurements for the corresponding load directions, response curves were plotted to highlight the nonlinearities in the system response for different load ranges.

The mainshaft displacements showed higher nonlinearity in the partial loads as compared to the full load region. The bedplate deformation identified by measuring the strains in the critical hot-spot regions showed a linear behavior for all load cases. Also, the gearbox roll tilt under the application of stepped torque loads exhibited a linear relationship. Such cases where the responses exhibit either a linear overall response or nonlinearity primarily within partial load regions are particularly well-suited for hybrid testing.

In contrast, the gearbox pitching and yawing tilts showed exponential relationships between applied loads and observed responses with higher nonlinearity at full loads. Gear flank load distribution demonstrated a decaying trend with increasing torque loads and an exponential growth trend with increasing pitching moments. Gearbox vibrations exhibited highly nonlinear characteristics in most locations and directions. A strong correlation was observed between these vibrations and gear flank load distribution under applied pitching moments, suggesting the influence of increased non-torque loads at higher pitching moment levels. Under applied torque, the gearbox vibrations displayed distinct nonlinear profiles across the three measured directions. With applied pitching moments, vibrations showed minimal change at partial loads but a rapid increase in the full load region across all three measured directions. Such responses can pose challenges for model validation using solely partial load measurements.

**Acknowledgements** The project VirtGondel was funded by the German Federal Ministry for Economic Affairs and Climate Action (BMWK) under the grant number 03EE2018. The authors would like to thank the involved colleagues at Fraunhofer IWES and GE Vernova for their contributions to the VirtGondel project.

**Funding** Open Access funding enabled and organized by Projekt DEAL.

## Declarations

**Conflict of interest** On behalf of all authors, the corresponding author states that there is no conflict of interest.



## References

1. Siddiqui MO, Feja PR, Borowski P, Kyling H, Nejad AR, Wenske J (2023) Wind Turbine Nacelle Testing: State-of-the-Art and Development Trends. Renewable and Sustainable Energy Reviews 188(4):113767. https://doi.org/10.1016/j.rser.2023.113767 (PII: S136403212300624X)
2. Duda T, Jacobs G, Bosse D (2016) IEA Wind Task 35 – Full Size Ground Testing of Wind Turbine Nacelles. Wind Europe Summit
3. Eustorgi K, Mechler S, Wegner A (2021) Comparison of wind turbine drive train loads measured in the field and on a nacelle test bench. In: Conference for Wind Power Drives, CWD 2021 : Extended Abstracts, pp 94–101
4. Siddiqui MO, Eustorgi K, Feja P (2024) Comparison of drivetrain vibration response during field operation and on a nacelle test bench. J Phys: Conf Ser 2767(4):42019. https://doi.org/10.1088/1742-6596/2767/4/042019
5. Jassmann U, Frehn A, Röttgers H, Santjer F, Mehler C, Beißel T, Kaven L, den Hoff D, Frühmann R, Azarian S, Neshati M, Quistorf G, Zuga A, Brennecke M, Jersch T, Schelenz R (2021) CertBench: conclusions from the comparison of certification results derived on system test benches and in the field. Forsch Ingenieurwes 85(2):353–371. https://doi.org/10.1007/s10010-021-00470-1 (PII: 470)
6. MEGAVIND Test and Demonstration Facilities for Wind Energy Needed to Promote a Competitive Wind Industry in Denmark. Technical report. https://megavind.winddenmark.dk/
7. Feja PR, Kyling H, Siddiqui MO, Wenske J Hybrides Prüfverfahren, Insbesondere Für Einen Antriebsstrang Von Windenergieanlagen. DE102022211558 A1, 2024. FRAUNHOFER GES FORSCHUNG. https://publica.fraunhofer.de/
8. Siddiqui MO, Nejad AR, Wenske J (2023) On a new methodology for testing full load responses of wind turbine drivetrains on a test bench. Forschung im Ingenieurwesen 87(1):173–184. https://doi.org/10.1007/s10010-023-00629-y (PII: 629)
9. Siddiqui MO, Nejad AR, Wenske J (2025) Establishing the Partial Load Limits for Main Shaft Response Prediction in Wind Turbine Hybrid Nacelle Testing. ([Manuscript submitted for publication])
10. Reisch S, Jacobs G, Bosse D, Loriemi A (2018) Experimental and Model-based Analysis of the Force Transmission in a Rotor Bearing Support System. J Phys: Conf Ser 1037:62028. https://doi.org/10.1088/1742-6596/1037/6/062028
11. Wenske J (2022) Nacelles, Drivetrains and Verification. Energy Engineering. Wind Turbine System Design, vol 1. Institution of Engineering and Technology, UK https://doi.org/10.1049/PBPO142F
12. Keller J, Guo Y, Zhang Z, Lucas D (2018) Comparison of planetary bearing load-sharing characteristics in wind turbine gearboxes. Wind Energy Sci 3(2):947–960. https://doi.org/10.5194/wes-3-947-2018

13. Guo Y, Keller J Validation of a Generalized Formulation for Load-Sharing Behavior in Epicyclic Gears for Wind Turbines. Technical Report NREL/CP-5000-76380, National Renewable Energy Laboratory. www.nrel.gov/publications
14. ISO 6336-1 (2015) Calculation of Load Capacity of Spur and Helical Gears—Part 1: Basic Principles, Introduction and General Influence Factors. Geneva, Switzerland
15. Irisarri JC, Santiago UG, Sison AF, Arce PO (2018) Load Intensity Distribution Factor Evaluation from Strain Gauges at the Gear Root. In: American Gear Manufacturers Association Fall Technical Meeting 2018. Curran Associates, Inc, Oak Brook, Illinois, USA, pp 154–175
16. Kock S, Jacobs G, Bosse D (2019) Determination of Wind Turbine Main Bearing Load Distribution. J Phys: Conf Ser 1222(1):12030. https://doi.org/10.1088/1742-6596/1222/1/012030
17. Guo Y, Bankestrom O, Bergua R, Keller J, Dunn M (2021) Investigation of Main Bearing Operating Conditions in a Three-Point Mount Wind Turbine Drivetrain. Forsch Ingenieurwes 85(2):405–415. https://doi.org/10.1007/s10010-021-00477-8 (PII: 477)
18. Matzke D, Schelenz R, Reisch S, Roscher B, Jacobs G, Theling J, Schroers M, Löpenhaus C, Brecher C (2018) Validation of the gearbox load calculation of a wind turbine MBS model. J Phys: Conf Ser 1037:62025. https://doi.org/10.1088/1742-6596/1037/6/062025
19. Guo Y, Keller J, Lacava W (2015) Planetary gear load sharing of wind turbine drivetrains subjected to non-torque loads. Wind Energy 18(4):757–768. https://doi.org/10.1002/we.1731
20. Li Z, Wen B, Peng Z, Dong X, Qu Y (2020) Dynamic modeling and analysis of wind turbine drivetrain considering the effects of non-torque loads. Appl Math Model 83:146–168. https://doi.org/10.1016/j.apm.2020.02.018 (PII: S0307904X20301037)